Event-Triggered Indirect Herding Control of a Cooperative Agent

Patrick M. Amy, Brandon C. Fallin, Jhyv N. Philor, and Warren E. Dixon, *Fellow, IEEE*

***Abstract*—This work explores the indirect herding control problem for a single pursuer agent regulating a single target agent to a goal location. To accommodate the constraints of sensing hardware, an event-triggered inter-agent influence model between the pursuer agent and target agent is considered. Motivated by fielded sensing systems, we present an event-triggered controller and trigger mechanism that satisfies a user-selected minimum inter-event time. The combined pursuer-target system is presented as a switched system that alternates between stable and unstable modes. A dwell-time analysis is completed to develop a closed-form solution for the maximum time the pursuer agent can allow the target agent to evolve in the unstable mode before requiring a control input update. The presented trigger function is designed to produce inter-event times that are upper-bounded by the maximum dwell time. The effectiveness of the proposed approach is demonstrated through both simulated and experimental studies, where a pursuer agent successfully regulates a target agent to a desired goal location.**

***Index Terms*—Autonomous robots, multi-robot systems, nonlinear control systems.**

I. Introduction

DEVELOPING a single robotic system that integrates a full navigation sensor suite (inertial navigation system, Doppler velocity log, ultra-short baseline sonar, etc.) alongside high-bandwidth communication hardware and all required mission payloads is often cost prohibitive. These challenges are further compounded by strict size, weight, and power constraints, as well as the need to support multiple mission types in complex and unpredictable environments. An agent with a robust sensor suite can leverage inter-agent interactions to provide navigation corrections to agents without state sensing capabilities. Agents without state sensing capabilities can optimize their form factor for mission-specific equipment, eliminating the need for extensive navigation and localization hardware. This concept of specialized agents with complementary capabilities connects to the pursuit-evasion paradigm, where different agents use sensor-based interaction to achieve complex objectives in challenging environments.

Received 24 July 2025; accepted 22 December 2025. Date of publication 9 February 2026; date of current version 17 February 2026. This article was recommended for publication by Associate Editor F. Miao and Editor M. A. Hsieh upon evaluation of the reviewers' comments. This work was supported in part by AFOSR under Grant FA9550-19-1-0169 and in part by AFOSR under Grant FA9550-21-1-0157. *(Corresponding author: Patrick Amy.)*

The authors are with the Department of Mechanical and Aerospace Engineering, University of Florida, Gainesville, FL 32611 USA (e-mail: patrick.amy@ufl.edu; brandonfallin@ufl.edu; jhyvphilor@ufl.edu; wdixon@ufl.edu).

Digital Object Identifier 10.1109/LRA.2026.3662559

The pursuit-evasion problem involves one or more pursuer agents attempting to intercept one or more target agents (also referred to as evader agents). In general, the target agents attempt to avoid interception by the pursuer agent (e.g., [1], [2], [3], [4]). When a target agent has the same goal as the pursuer agent, the target agent is referred to as cooperative [5], [6], [7]. When a target agent does not have a goal, or has a different goal from the pursuer agent(s), then the target agent is deemed non-cooperative [5], [6], [7].

Indirect control, also called herding, is a type of pursuit-evasion problem that differs from standard pursuit-evasion results because indirect control includes regulating the target agent to a control objective (e.g., goal location, velocity alignment, or desired trajectory) after interception [8]. Indirect control makes use of an inter-agent influence model (also referred to as an interaction model), allowing one agent to control another agent (e.g., [5], [6], [7], [8], [9], [10], [11], [12], [13], [14], [15], [16]). For example, the results in [8] and [11] characterize inter-agent interactions through relative displacement functions between pursuing and target agents. Specifically, the target agent in [8] and [11] moves directly away from pursuer agent based on the relative displacement between the two agents. The inter-agent interaction was incorporated into the pursuer agent's control design to effectively regulate the target agent to a goal location. In [16], the authors present an algorithm for indirectly controlling a swarm of agents using bearing-only measurements. The results in [16] can be considered a heuristic approach for generating pursuer trajectories, whereas this work uses a control theoretic approach to guarantee system convergence that is influenced by a zero-order hold relative direction inter-agent influence function.

The herding problem has been examined across multiple disciplines with the findings typically categorized into two main approaches: control theoretic methods (e.g., [5], [6], [8], [11]) and rule-based methods (e.g., [17], [18], [19], [20]). Alternatively, some results make use of machine learning, leveraging offline training to heuristically learn inter-agent interactions to achieve herding or fulfill a rule-based method (e.g., [18], [19], [20]). Control theoretic methods involve developing feedback control strategies to drive the pursuer to regulate the state of the target agent to a desired set-point (e.g., [5], [7], [10], [14], [15], [21]). Learning-based and rule-based methods can be grouped together because their results take a similar form and they are both limited to relatively small flock sizes. These limitations have motivated the use of control theoretic methods, where a

2377-3766 © 2026 IEEE. All rights reserved, including rights for text and data mining, and training of artificial intelligence and similar technologies. Personal use is permitted, but republication/redistribution requires IEEE permission. See https://www.ieee.org/publications/rights/index.html for more information.

Authorized licensed use limited to: University of Florida. Downloaded on February 17,2026 at 23:10:35 UTC from IEEE Xplore. Restrictions apply.

single pursuer agent indirectly controls larger flocks (e.g., [17], [18], [19], [20], [22]).

Event-triggered control (ETC) offers clear advantages to address energy, computation, and communication constraints when designing feedback control laws for multi-agent systems [23], [24], [25], [26], [27]. ETC involves feedback control updates that occur in non-uniform time intervals [24]. ETC methods are comprised of two elements: a feedback controller that computes the control input, and a trigger function that dictates when to update the control input [24]. In ETC, the trigger function (also called a trigger mechanism or trigger generator) is typically a function of the system state, requiring periodic sampling for updates [23], [28]. ETC results typically employ a zero-order hold control law, where an agent's control input is held constant between updates (e.g., [24], [28], [29]). When an event-trigger condition is met an event occurs, and the time when the event happens is called an event time [30]. The difference between consecutive event times is called the inter-event time (IET). The minimum IET is defined as the lower bound on the IETs, and the maximum IET is defined as the upper bound on the IETs [30]. It is necessary to show that switching systems do not exhibit Zeno behavior. Zeno behavior occurs when a process experiences infinitely many discrete transitions in a finite time duration and is not implementable on physical systems [30], [31], [32].

ETC facilitates the investigation of indirect control applications where low-frequency sensors are employed. Indirect control results such as [5], [6], [7], [8], [10], [11], [12], [13], [14], [15], [33], [34], [35] consider a perpetual interaction model between the pursuer agent and target agent, where pursuer agents and target agents are in continuous sensing and control engagement. This work is the first to consider an intermittent interaction model that allows the target agent to sense the pursuer agent at discrete intervals. Furthermore, unlike results such as [8], [11], [12], [35], this is the first work that considers a target agent that maintains a constant speed without stopping, loitering, or meandering when the pursuer is absent. The constant speed of the target agent creates a lower bound on the convergence time, constraining the time available for a pursuer agent to regulate the target agent to a goal. Results such as [8], [11], [12], [35] focus on scenarios in which one pursuer agent regulates multiple target agents. Such results use switched system analyses to develop dwell-time criteria that determine how long a pursuer agent is permitted to engage a target agent before switching to another target agent.

Without considering a maximum target agent speed, prior results permit a pursuer agent to regulate a target agent to the goal within the prescribed dwell time. Thus, the pursuer agent does not need to switch to regulate a different target agent until the current target agent has been sufficiently stabilized. In this work, the combined pursuer-target system is analyzed as a switched system that alternates between stable and unstable modes. Additionally, in this work, the pursuer agent intermittently imparts an influence onto the target agent. Given the constant speed of the target agent and the intermittent influence from the pursuer, the system must evolve in the unstable mode for a non-negligible duration before transitioning back to the stable mode. This constraint led to unique challenges in ensuring overall system convergence and stability, which were remedied by the design of the trigger function. This work develops a new approach for understanding intermittent interaction dynamics, broadening the applicability of indirect control applications.

In this work, a pursuer agent regulates (herds) a cooperative target agent towards a goal location through a relative bearing interaction function. We leverage a Lyapunov-based stability analysis to establish stability criteria, ensuring the proposed control law guarantees target agent regulation to a desired state. We develop a closed-form solution for the maximum IET via a dwell-time analysis, which is then integrated into a piecewise continuous trigger function. The designed trigger function incorporates a user-defined minimum IET, which inherently prevents Zeno behavior since the minimum IET is strictly greater than zero. The maximum IET can be computed *a priori*, providing a tunable parameter that allows the user to balance control responsiveness and efficiency. This configurability ensures that the maximum IET can be made sufficiently large to accommodate a desired minimum IET while achieving the control objective. To validate the developed approach, we present both a simulated and an experimental study demonstrating successful regulation of a target agent to a goal location by a pursuer agent, showcasing the effectiveness and practical applicability of our method.

II. Preliminaries

A. Notation

The set of real numbers and integers are represented by $\mathbb{R}$ and $\mathbb{Z}$, respectively. For a real number $a \in \mathbb{R}$, let the set of real numbers greater than and strictly greater than a be represented by $\mathbb{R}_{\geq a} \triangleq [a, \infty)$ and $\mathbb{R}_{>a} \triangleq (a, \infty)$, respectively. Similarly, the set of integers greater than and strictly greater than a are defined as $\mathbb{Z}_{\geq a} \triangleq \mathbb{R}_{\geq a} \cap \mathbb{Z}$ and $\mathbb{Z}_{>a} \triangleq \mathbb{R}_{>a} \cap \mathbb{Z}$, respectively. The Euclidean norm of a vector $u \in \mathbb{R}^n$ is denoted by $\|u\| \triangleq \sqrt{u^\top u}$. The inner product of two vectors $u, v \in \mathbb{R}^n$ is denoted $\langle u, v \rangle \triangleq u^\top v$.

III. Problem Formulation

A single pursuer agent is tasked with regulating a single cooperative target agent to a goal location, which is unknown to the target agent. Unlike results such as [5], [8], [11], the target agent is only capable of measuring the relative direction to the pursuer agent when dictated by the pursuer agent's trigger function. Let $\eta_t(t) : \mathbb{R}_{\geq 0} \to \mathbb{R}^n$ denote the target agent's position, and let $\eta_p(t) : \mathbb{R}_{\geq 0} \to \mathbb{R}^n$ denote the pursuer agent's position. The dynamics of the target agent are given by

$$\dot{\eta}_t(t) \triangleq f\left(\eta_t(t)\right) + \mu_t\left(\eta_t\left(t_k\right), \eta_p\left(t_k\right)\right) \tag{1}$$

where the zero-order hold inter-agent influence is denoted $\mu_t(\eta_t(t_k), \eta_p(t_k)) : \mathbb{R}^n \times \mathbb{R}^n \to \mathbb{R}^n$, t_k denotes the k^{th} time instant when the pursuer agent influences the target agent, and $f : \mathbb{R}^n \to \mathbb{R}^n$ represents the target agent's unknown drift

Authorized licensed use limited to: University of Florida. Downloaded on February 17,2026 at 23:10:35 UTC from IEEE Xplore. Restrictions apply.

dynamics. The inter-agent influence function is defined by

$$\mu_t\left(\eta_t\left(t_k\right),\eta_p\left(t_k\right)\right) \triangleq \begin{cases} \nu_t\left(\frac{\eta_t(t_k)-\eta_p(t_k)}{\|\eta_t(t_k)-\eta_p(t_k)\|}\right), \\ \quad \text{if } \|\eta_t\left(t_k\right)-\eta_p\left(t_k\right)\| \le R_p \\ 0, \quad \text{otherwise}, \end{cases} \tag{2}$$

where $\nu_t \in \mathbb{R}_{>0}$ denotes the constant speed of the target agent and $R_p \in \mathbb{R}_{>0}$ denotes the known maximum distance at which the pursuer agent can exert influence over the target agent. The influence function in (2) defines a unit vector from the pursuer to the target, scaled by the target's constant speed. This influence function denotes the effect of the pursuer's position on the target's velocity during influence events. Furthermore, the influence function in (2) is motivated by sensor applications in which sensing can only occur between discrete time intervals. The use of a relative direction influence is motivated by a sensor such as an underwater SONAR, which motivates the inclusion of a maximum influence range. The target agent's dynamics are not directly controllable; therefore, the pursuer agent will regulate the target agent's trajectory by positioning itself to update the zero-order hold influence function in (2). Unlike the target agent, the pursuer agent is directly controllable with dynamics

$$\dot{\eta}_p(t) \triangleq \mu_p(t), \tag{3}$$

where $\mu_p(t) : \mathbb{R}_{>0} \to \mathbb{R}^n$ denotes the control input of the pursuer agent.

Assumption 1: The target agent's drift dynamics, $f : \mathbb{R}^n \to \mathbb{R}^n$, are continuously differentiable and bounded as $\|f(\eta_t(t))\| \le \overline{f}$.

Assumption 2: The pursuer agent can continuously measure its state, $\eta_p(t)$, and the target agent's state, $\eta_t(t)$ for all $t \in \mathbb{R}_{\ge 0}$.

Assumption 3: The pursuer agent can instantaneously impart influence on the target agent defined by the inter-agent influence function in (2).

Remark 1: Assumptions 1–3 represent idealized conditions that enable the theoretical Lyapunov convergence analysis. In practice, sensing of target and pursuer agent states occurs at discrete time intervals rather than continuously, and the propagation of the inter-agent influence signal experiences delays rather than being instantaneous. The minimum IET parameter $\delta_{\min}$ provides a mechanism to accommodate these practical limitations. Selecting $\delta_{\min}$ larger than the combined sensing period and actuation delay enables the theoretical framework to be applied to real-world systems. The conservative bound of the norm of the target agent's drift dynamics denoted by $\overline{f}$ further provides safety margins in the maximum IET.

IV. Control Objective

The goal of the pursuer agent is to regulate the target agent's state to a static desired goal location, $\zeta_g \in \mathbb{R}^n$. To quantify the target agent regulation objective, the target agent position error $e_t(t) : \mathbb{R}_{\ge 0} \to \mathbb{R}^n$ is defined as

$$e_t(t) \triangleq \eta_t(t) - \zeta_g. \tag{4}$$

The pursuer agent error $e_p(t) : \mathbb{R}_{\ge 0} \to \mathbb{R}^n$, is defined as

$$e_p(t) \triangleq \eta_d(t) - \eta_p(t), \tag{5}$$

where $\eta_d(t) : \mathbb{R}_{\ge 0} \to \mathbb{R}^n$ represents the pursuer agent's desired trajectory, which is defined as

$$\eta_d(t) \triangleq \eta_t(t) + R_a S_0, \tag{6}$$

where $S_0 \triangleq -e_t(t)/\|e_t(t)\|$ denotes a direction vector equal to the normalized direction from the goal location to the target agent, and $R_a \in \mathbb{R}_{>0}$ represents the desired influence range, where R_a must be selected such that $R_a \le R_p$. The minimum and maximum influence ranges are motivated by the pursuer agent's use of sensors to influence the target agent's control input. Based on the subsequent stability analysis, the pursuer agent's controller is designed as

$$\mu_p(t) \triangleq \dot{\eta}_d(t) + (\beta+1)\, e_p(t) \tag{7}$$

where $\beta \in \mathbb{R}_{>0}$ is a user-selected constant. In the following subsection, we formulate a trigger function that determines conditions under which the pursuer agent exerts influence on the target agent's trajectory.

A. Trigger Design

The pursuer agent influences the target agent when dictated by the trigger function $T : \mathbb{R} \times \mathbb{R}^n \times \mathbb{R}^n \to \mathbb{R}$. The minimum and maximum IETs are denoted by $\delta_{\min}$ and $\delta_{\max}$, respectively. The trigger function is designed to incorporate a user-prescribed minimum IET to account for sensing or communication constraints. The trigger function employs a timer, $\tau \in \mathbb{R}_{>0}$, to enforce the minimum and maximum IETs while allowing elements of the system state to dictate events between the maximum and minimum IET limits. The timer is described by $\tau \triangleq t - t_k$, where t_k is the time the last influence event occurred. The trigger function is defined as

$$T \triangleq \begin{cases} \gamma_s, & \tau < \delta_{\min}, \\ \gamma_s + \|e_p(t)\|^2 - (\alpha+1)\,\|e_t(t)\|^2, & \delta_{\min} \le \tau < \delta_{\max}, \\ 0, & \text{otherwise}, \end{cases} \tag{8}$$

where $\gamma_s \triangleq \frac{1}{2}\overline{f}^2 + \frac{1}{2}{\nu_t}^2 + (\alpha+1)\|e_t(t_k)\|^2$ and $\alpha \in \mathbb{R}_{>0}$ is a user-defined constant. When $\tau < \delta_{\min}$, the trigger function is a positive constant equal to γ_s, preventing the pursuer agent from influencing the target agent before the minimum IET condition has been met. When the timer τ is between the minimum and maximum IETs, we have $\delta_{\min} \le \tau < \delta_{\max}$ and the trigger function T is dependent on the system error signals $e_p(t)$ and $e_t(t)$. When the timer is equal to the maximum IET, the trigger function is set to zero. The trigger function generates an influence event when $T = 0$. This condition can occur when the timer reaches the maximum IET or if the norm of the target agent error, $\|e_t\|$, grows sufficiently large. From (8), since $T = \gamma_s$ when $\tau < \delta_{\min}$, the pursuer agent cannot influence the target agent when the IETs are less than the minimum IET. Therefore, Zeno behavior is prevented given the minimum IET is selected such that $\delta_{\min} \in$

Authorized licensed use limited to: University of Florida. Downloaded on February 17,2026 at 23:10:35 UTC from IEEE Xplore. Restrictions apply.

$(0, \delta_{\max}]$. When $T = 0$, the k^{th} influence time is updated as $t_k = t$ and the timer τ is reset such that $\tau = 0$. Additionally, the constant γ_s is reset to $\gamma_s = \frac{1}{2}\overline{f}^2 + \frac{1}{2}{\nu_t}^2 + (\alpha+1)\|e_t(t_k)\|^2$. The trigger function can be constructed to rely only on a timer variable; however, including the error signal component allows the trigger function to generate influence events more often if the target is not tracking the desired trajectory. That is, the error signal component of T enables influence events to occur before $\tau = \delta_{\max}$.

The minimum IET, $\delta_{\min}$, serves a dual purpose; preventing Zeno behavior as proven in the subsequent theoretical analysis, and accommodating practical sensing and actuation constraints in implementation. By selecting $\delta_{\min} > T_{sense} + T_{\text{delay}}$, where T_{sense} is the sensing period and T_{delay} is the actuation delay, the user can ensure the framework remains implementable on real hardware.

The maximum IET, $\delta_{\max}$, derived from the switched systems stability analysis, (25), represents the longest permissible time the target agent can remain in the unstable subsystem before convergence guarantees are compromised. Unlike $\delta_{\min}$, which addresses hardware constraints, $\delta_{\max}$ emerges from the underlying dynamics of the target-pursuer system and ensures convergence of the target agent's position to the goal location.

V. Stability Analysis

The stability analysis considers the system in two parts: a converging subsystem when the pursuer agent influences the target agent, and a diverging subsystem when the pursuer agent does not influence the target agent. After each subsystem is considered independently, stability criteria are developed by considering the combined system as a switched system. For notational brevity, the time dependence of functions and variables is omitted in the following analysis, unless additional clarity is required. In the following subsections, t_k^s and t_k^u represent the k^{th} time instant the combined system enters its stable and unstable subsystem, respectively. Specifically, the sequence t_k^s, t_k^u, t_{k+1}^s represents an iteration of entering the stable subsystem for the k^{th} time, followed by the unstable subsystem for the k^{th} time, followed by stable subsystem for the $(k+1)^{\text{th}}$ time. From Assumption 3, $t_k^u - t_k^s = 0$. Therefore, in (8), $t_k = t_k^u$ and the trigger function evolves while in the unstable subsystem. Let $\xi = [e_p^\top, e_t^\top]^\top : \mathbb{R}_{\geq 0} \to \mathbb{R}^{2n}$ represent the concatenated vector of agent regulation errors. Consider the common candidate Lyapunov function, $V : \mathbb{R}^{2n} \to \mathbb{R}$,

$$V(\xi) = \frac{1}{2} e_p^\top e_p + \frac{1}{2} e_t^\top e_t. \tag{9}$$

A. State Convergence

The following stability analysis reveals that all system trajectories converge to the set $\mathcal{B} \triangleq \{\xi \in \mathbb{R}^{2n} : \|\xi(t)\|^2 \leq \frac{\gamma_s}{\lambda_s}\}$, where $\lambda_s \triangleq \min\{\beta, \alpha\}$ determines the rate of convergence, establishing globally uniformly ultimately bounded (UUB) regulation.

Theorem 1: For the dynamical systems in (1) and (3) and any initial state $\xi(t_0)$, the control law given in (7) ensures $\xi(t)$ converges exponentially to the set $\mathcal{B}$, where

$$\|\xi(t)\|^2 \leq \left(\|\xi(t_k^s)\|^2 - \frac{\gamma_s}{\lambda_s}\right) e^{-2\lambda_s\left(t - t_k^s\right)} + \frac{\gamma_s}{\lambda_s} \tag{10}$$

for all $t \in [t_k^s, t_k^u)$, given that $\alpha > 0$, $\beta > 0$, and Assumptions 1–3 are satisfied.

Proof: Taking the total derivative of (9) along the trajectories of ξ, and substituting the dynamics of the target agent from (1) and the time derivative of (5) yields

$$\dot{V}(\xi) = e_p^\top (\dot{\eta}_d - \dot{\eta}_p) - e_t^\top (f(\eta_t) + \mu_t). \tag{11}$$

Substituting (3) and (7) into (11) yields

$$\dot{V}(\xi) = -\beta e_p^\top e_p - e_t^\top (f(\eta_t) + \mu_t). \tag{12}$$

Using the Cauchy-Schwarz inequality and Young's inequality, (12) can be written as

$$\dot{V}(\xi) \leq -\beta \|e_p\|^2 + \|e_t\|^2 + \frac{1}{2}\|f(\eta_t)\|^2 + \frac{1}{2}\|\mu_t\|^2. \tag{13}$$

Given $\|f(\eta_t(t))\| \leq \overline{f}$ and $\|\mu_t\| \leq \nu_t$, we can upper bound (13) as

$$\dot{V}(\xi) \leq -\beta \|e_p\|^2 + \|e_t\|^2 + \frac{1}{2}\overline{f}^2 + \frac{1}{2}\nu_t^2. \tag{14}$$

Since $\gamma_s = \frac{1}{2}\overline{f}^2 + \frac{1}{2}{\nu_t}^2 + (\alpha+1)\|e_t\|^2$ while $t \in [t_k^s, t_k^u)$, then (14) can be expressed as

$$\begin{aligned}\dot{V}(\xi) \leq &-\beta \|e_p\|^2 + \|e_t\|^2 \\ &+ \gamma_s - (\alpha+1)\|e_t\|^2.\end{aligned} \tag{15}$$

Therefore, (15) becomes

$$\dot{V}(\xi) \leq -\beta \|e_p\|^2 - \alpha \|e_t\|^2 + \gamma_s \tag{16}$$

Using the fact that $\lambda_s = \min\{\beta, \alpha\}$ and substituting (9) into (16) yields

$$\dot{V}(\xi) \leq -2\lambda_s V(\xi) + \gamma_s. \tag{17}$$

Solving the differential inequality in (17) yields

$$\begin{aligned}V(\xi(t)) \leq &V(\xi(t_k^s))\, e^{-2\lambda_s\left(t - t_k^s\right)} \\ &+ \frac{\gamma_s}{2\lambda_s}\left(1 - e^{-2\lambda_s\left(t - t_k^s\right)}\right).\end{aligned} \tag{18}$$

Using [36, Def. 4.6] shows that ξ is uniformly ultimately bounded by

$$\|\xi(t)\| \leq \sqrt{\|\xi(t_k^s)\|^2 e^{-2\lambda_s\left(t - t_k^s\right)} + \frac{\gamma_s}{\lambda_s}\left(1 - e^{-2\lambda_s\left(t - t_k^s\right)}\right)},$$

for all $t \in [t_k^s, t_k^u)$, which yields the result in (10). ■

B. State Divergence

Theorem 2: For the dynamical systems in (1) and (3) and $t \in [t_k^u, t_{k+1}^s)$, the state $\xi(t)$ remains bounded as

$$\|\xi(t)\|^2 \leq \left(\|\xi(t_k^u)\|^2 + \gamma_u\right) e^{2\left(t - t_k^u\right)} - \gamma_u, \tag{19}$$

where $\gamma_u \in \mathbb{R}_{>0}$ is defined as $\gamma_u \triangleq \frac{1}{2}\overline{f}^2 + \frac{1}{2}{\nu_t}^2 \in \mathbb{R}_{>0}$.

Authorized licensed use limited to: University of Florida. Downloaded on February 17,2026 at 23:10:35 UTC from IEEE Xplore. Restrictions apply.

Proof: Taking the total derivative of (9) along trajectories of ξ, substituting the dynamics of the target agent from (1), and substituting the time derivative of (5) yields

$$\dot{V} = e_p^\top \left(\dot{\eta}_d - \dot{\eta}_p\right) + e_t^\top \left(f\left(\eta_t\right) + \mu_t\right). \tag{20}$$

Substituting (3) and (7) into (20) yields

$$\dot{V} = e_p^\top \left(\dot{\eta}_d - \left(\dot{\eta}_d + \beta e_p\right)\right) + e_t^\top \left(f\left(\eta_t\right) + \mu_t\right). \tag{21}$$

Using the Cauchy-Schwarz inequality, Young's inequality, and Assumption 1, (21) is upper-bounded as

$$\dot{V} \leq -\beta \left\|e_p\right\|^2 + \left\|e_t\right\|^2 + \frac{1}{2}\overline{f}^2 + \frac{1}{2}{\nu_t}^2. \tag{22}$$

Given $-\beta\|e_p\|^2 \leq \|e_p\|^2$ and $\gamma_u = \frac{1}{2}\overline{f}^2 + \frac{1}{2}{\nu_t}^2$, we can further bound (22) as

$$\dot{V} \leq 2V + \gamma_u. \tag{23}$$

Solving the differential inequality in (23) yields

$$V(t) \leq V\left(t_k^u\right) e^{2\left(t - t_k^u\right)} + \frac{1}{2}\gamma_u \left(e^{2\left(t-t_k^u\right)} - 1\right), \tag{24}$$

for all $t \in [t_k^u, t_{k+1}^s)$. Substituting (9) into (24) and simplifying the expression yields the result in (19). ■

C. Combined Stability Analysis

Theorem 3: The combination of the trigger function in (8) and the control law in (7) guarantees that the state ξ remains bounded by

$$\|\xi(t)\|^2 \leq \left(\|\xi\left(t_k^s\right)\|^2 - \frac{\gamma_s}{\lambda_s}\right) e^{-2\lambda_s\left(t - t_k^s\right)} + \frac{\gamma_s}{\lambda_s}$$

for all $t \in \mathbb{R}_{\geq 0}$ given that $t_{k+1}^s - t_k^u < \delta_k$ and

$$\delta_k \leq \frac{1}{2}\ln\left[\frac{\xi_s + \gamma_u}{\xi_u}\right], \tag{25}$$

where $\xi_s \triangleq \|\xi(t_k^s)\|^2$, and $\xi_u \triangleq \|\xi(t_k^u)\|^2$.

Proof: The stable subsystem is upper-bounded by (10), which can be written as

$$\|\xi(t)\| \leq \sqrt{\left(\xi_s - \frac{\gamma_s}{\lambda_s}\right) e^{-2\lambda_s\left(t - t_k^s\right)} + \frac{\gamma_s}{\lambda_s}}. \tag{26}$$

The unstable subsystem is bounded by (19), which can also be written as

$$\|\xi(t)\| \leq \sqrt{\left(\xi_u + \gamma_u\right) e^{2\left(t - t_k^u\right)} - \gamma_u}. \tag{27}$$

Since the influence updates occur instantaneously, $t_{k+1}^u - t_k^s = 0$, and the system predominantly remains in the unstable subsystem. The time interval $\delta_k = t_{k+1}^s - t_k^u$ is the time interval from when the system enters the unstable subsystem until it exits the unstable subsystem. Consider the unstable subsystem in δ_k and the stable subsystem in the preceding interval $\delta_{k-1} = t_k^u - t_k^s$. Given that the influence the pursuer imparts on the target agent occurs instantaneously, then $\delta_{k-1} = 0$. Let the unstable subsystem be bounded by the stable subsystem, then (26) and (27) can be expressed as

$$\xi_u e^{2\delta_k} \leq \left(\xi_s - \frac{\gamma_s}{\lambda_s}\right) e^{-2\lambda_s \delta_{k-1}} + \frac{\gamma_s + \lambda_s\gamma_u\left(1 - e^{2\delta_k}\right)}{\lambda_s}. \tag{28}$$

Since $\delta_{k-1} = 0$, (28) can be bounded by

$$\xi_u e^{2\delta_k} \leq \xi_s + \gamma_u. \tag{29}$$

Solving for δ_k in (29) yields the result in (25). ■

Remark 2: During the interval $t \in [t_k^s, t_k^u)$, the radius of the set $\mathcal{B}$ decreases because the target agent converges toward the goal location. Conversely, the radius of the set $\mathcal{B}$ expands when the target agent diverges from the goal location during this same interval. The evolution of the radius of $\mathcal{B}$ occurs because $\gamma_s = \frac{1}{2}\overline{f}^2 + \frac{1}{2}{\nu_t}^2 + (\alpha+1)\|e_t(t_k^s)\|^2$ is reset after each trigger event. Specifically, if $\|e_t(t_k^s)\| > \|e_t(t_{k-1}^s)\|$ then the radius of the set $\mathcal{B}$ increases, and if $\|e_t(t_k^s)\| < \|e_t(t_{k-1}^s)\|$ then the radius of the set $\mathcal{B}$ decreases. The trigger function given by (8) will generate influence events more frequently if the radius of $\mathcal{B}$ is growing due to target agent divergence from the goal location. When the target agent is diverging from the goal location, $\gamma_s + \|e_p(t)\|^2 - (\alpha+1)\|e_t(t)\|^2 = 0$ before $t - t_k = \delta_{\max}$, and the IETs will approach the minimum IET. Sections V-A and V-C imply that with each successive sequence $\delta_k \to \delta_{k+1}$, the radius of $\mathcal{B}$ decreases as the pursuer agent regulates the target agent to the goal. Furthermore, from the stability result, the radius of the set $\mathcal{B}$ decreases with each successive sequence $\delta_k \to \delta_{k+1}$, and $\limsup_{t\to\infty}\|\xi(t)\|^2 \leq \frac{1}{2\lambda_s}(\overline{f}^2 + {\nu_t}^2)$ for all $t \in [0, \infty)$.

VI. Results

A. Simulated Results

Numerical experiments demonstrate the efficacy of the controller in (7) and the trigger function in (8). The minimum IET $\delta_{\min}$ is determined by the sensing hardware constraints of the pursuer and target agents (e.g., the sampling time or processing time of the sensor). In this simulation study, the target agent drift dynamics are given by $f(\eta_t(t)) = \tanh(\eta_t(t))$, satisfying Assumption 1. For this simulation, we select $\delta_{\min} = 0.1 \cdot \delta_{\max}$, $n = 2$, $R_p = 10.0$, $R_a = 5.0$, $\nu_t = 1.5$, $\alpha = 2.1$, and $\beta = 5.0$. Based on the parameter selection, γ_u was found to be $\gamma_u = 1.9639$. Given the initial configuration represented by the ⊙'s in Fig. 1 and the value of γ_u, the maximum IET was found to be $\delta_{\max} = 0.178$ using 25. In Fig. 3, T increases during the interval $t - t_k < \delta_{\max}$ because the target agent's tracking error e_t diminishes as it approaches the goal location. If instead the tracking error were to increase during this period, T would rapidly decrease to zero closer to the minimum IET, $\delta_{\min}$. This relationship is critical for system efficiency—when T is driven to zero shortly after $\delta_{\min}$, the pursuer must intervene more frequently, indicating that the influence function is not effectively managing the target agent's tracking performance given the target agent's drift dynamics. The conservative nature of the result is evidence in Fig. 2, where it can be seen that the target agent's error does not grow between influence events. Based on the fact that the target agent's error does not grow in between influence events, it is possible for the maximum dwell

Authorized licensed use limited to: University of Florida. Downloaded on February 17,2026 at 23:10:35 UTC from IEEE Xplore. Restrictions apply.

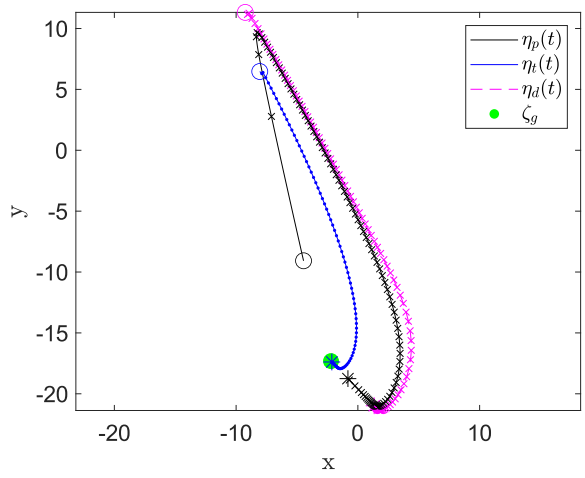

Fig. 1. The trajectories of the pursuer agent, $\eta_p(t)$, and target agent, $\eta_t(t)$, are represented by the black and blue lines respectively. The desired trajectory, $\eta_d(t)$, is represented by the magenta dashed line. The black and magenta $\times$'s represent $\eta_p(t_k)$ and $\eta_d(t_k)$ when $T = 0$. The blue solid dots represent $\eta_t(t_k)$ when $T = 0$. The black, magenta, and blue $\circledcirc$'s represent $\eta_p(t_0)$, $\eta_d(t_0)$, and $\eta_t(t_0)$. The $\star$'s represent $\eta_p(t_{\text{final}})$, $\eta_d(t_{\text{final}})$, and $\eta_t(t_{\text{final}})$. The green square represents the goal location.

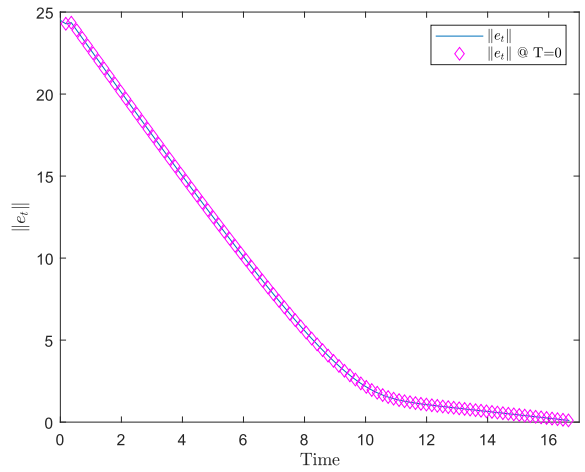

Fig. 2. The value of $\|e_t\|$ over time. The magenta $\diamondsuit$'s represent when the pursuer agent influences the target agent.

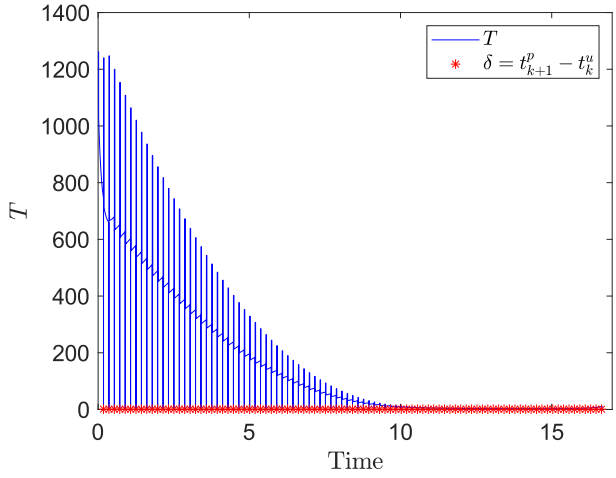

Fig. 3. The evolution of the trigger function, denoted by the blue line over time. Event times when the pursuer agent exerts influence on the target agent are marked with red $\star$'s. It can be seen that T resets to a constant and remains constant while $t^p_{k+1} - t^u_k \leq \delta_{\min}$. When $\delta_{\min} \leq t^p_{k+1} - t^u_k < \delta_{\max}$, T grows because $\|e_t\|^2$ gets smaller as the target agent is influenced in the direction of ζ_g. Finally, T is forced to zero when $t^p_{k+1} - t^u_k = \delta_{\max}$, which is evidenced by the downward spike at most red $\star$'s.

Fig. 4. The Freefly Astro quadcopter (left) was used as the pursuer agent and the Unitree Go1 quadruped (right) was used as the target agent. The quadruped uses an Emlid RS+ RTK GPS for precise position updates, which is fused with attitude and heading data from a Microstrain 3DM-GX5-AHRS using the ROS2 `robot_localization` package.

time to be increased while still ensuring the regulation of the target agent to the goal location.

B. Experiment

Experiments were performed at the University of Florida's Autonomy Park outdoor facility to validate the efficacy of the controller in (7) and the trigger function in (8). The results of a single experimental run are presented in Figs. 5 and 6. The experiment was carried out using the Freefly Astro and Unitree Go1 platforms shown in Fig. 4. In the experimental results, a pursuer agent (Freefly Astro quadcopter) was tasked with regulating a target agent (Unitree Go1 quadruped) to the desired coordinates $(-2.0\,\text{m}, -5\,\text{m}, 0\,\text{m})$ in the local Autonomy Park reference frame. The minimum IET, $\delta_{\min}$, was selected as 0.01 s. Based upon the documented tolerances of onboard sensors and the maximum velocity of the target agent, $\overline{f}$ was conservatively estimated to be 6.0 m/s. The target agent velocity, ν_t, was selected as 0.25 m/s. From (25), and based on the initial values of ξ_u and ξ_s, the maximum IET, $\delta_{\max}$, was computed to be 0.0282 s. The smallest and largest IETs from the experimental data were found to be 0.0154 s and 0.0248 s, respectively. Due to the small IETs, the influence and event markers shown in the simulation Figs. 1–3 were omitted from Figs. 5 and 6.

The experimental results demonstrate the effectiveness of the controller in (7) and the trigger function in (8), as the pursuer agent successfully regulated the target agent while maintaining IETs within the theoretically predicted bounds. In contrast to the

Authorized licensed use limited to: University of Florida. Downloaded on February 17,2026 at 23:10:35 UTC from IEEE Xplore. Restrictions apply.

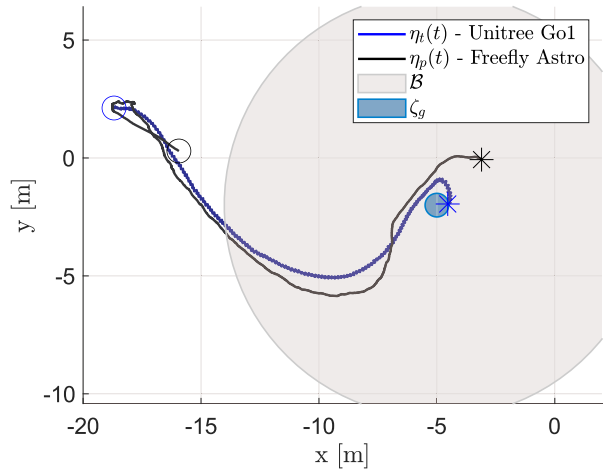

Fig. 5. The trajectories of the pursuer agent, $\eta_p(t)$, and target agent, $\eta_t(t)$, are represented by the black and blue lines respectively. The ◎'s represent $\eta_p(t_0)$ and $\eta_t(t_0)$. The ⋆'s represent $\eta_p(t_{\text{final}})$ and $\eta_t(t_{\text{final}})$. The light blue circle represents the goal location and the ultimate bound of $\mathcal{B}$ described in Remark 2 is depicted by the light gray circle.

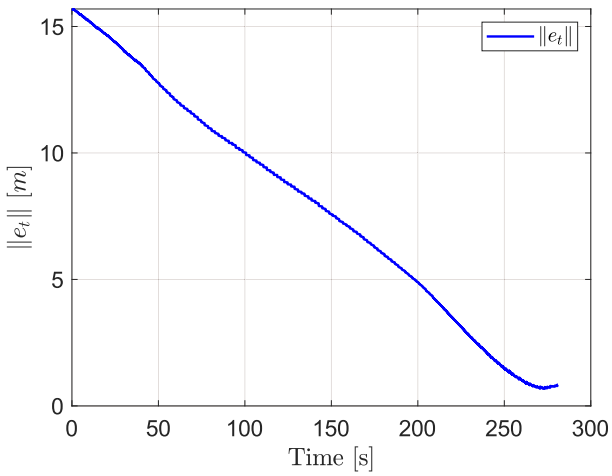

Fig. 6. The value of $\|e_t\|$ during the experiment. Notable changes in the slope correspond to effective regulation of the target agent's trajectory by the pursuer agent's movement patterns.

simulated results in Section VI-A, experimental results revealed that trigger events were primarily initiated by state conditions rather than timer constraints, demonstrating the system's efficient adaptation to the target agent's dynamic movements.

The experimental platform employs RTK GPS to provide precise position data of the target agent for the pursuer agent's control input and for ground truth validation of the theoretical framework. In operational scenarios, the target agent would rely on a minimal sensor suite for its localization (e.g., bearing-only measurements to the pursuer), while the pursuer agent maintains the high-fidelity localization capability. The bearing-based sensing model in (2) reflects this intended deployment framework.

VII. Conclusion

This work introduces a novel solution to the indirect control problem by leveraging an event-triggered relative bearing influence function to regulate a target agent toward a desired location. It is the first result to establish a rigorous connection between the maximum dwell time and IET bounds in an event-triggered indirect control framework. By formulating the system as a switched dynamical model with stable and unstable subsystems, this work develops a comprehensive dwell-time analysis to derive an upper bound on inter-event times for the trigger function. A piecewise continuous trigger function is proposed, incorporating both a maximum IET, determined through a dwell-time analysis, and a selectable minimum IET, providing enhanced control flexibility. Future research directions include the development of bounded control laws for pursuer agents to enable a closed-form solution of the minimum IET, and the extension of these analytical results to the bearing-only measurement case. Implementing a bearing-only measurement solution would eliminate the need for expensive positioning systems to obtain the position of the target agent, enabling the use of lower-cost target platforms than those used in the experimental validation of this work. Additionally, future work will explore the scalability of this approach to scenarios with multiple pursuer agents and target agents.

While the outdoor experiment demonstrates practical feasibility, we acknowledge that formal convergence guarantees under sensing noise, actuation delays, and asynchronous measurements require further theoretical development. Future work will involve incorporating stochastic measurement models into the switched systems analysis. Future contributions will require the derivation of explicit bounds on allowable sensing delays and actuation noise levels. An effective implementable result could be realized by developing robust trigger functions that formally account for the imperfections in sensing and actuation.

Acknowledgment

The authors would like to thank Dr. William Warke for his extensive efforts troubleshooting experimental hardware and solving critical software problems. His technical expertise and unwavering dedication were instrumental in ensuring the successful completion of this research project.

References

[1] J. P. Hespanha, Z. Dodds, G. D. Hager, and A. S. Morse, "What tasks can be performed with an uncalibrated stereo vision system?," *Int. J. Comput. Vis.*, vol. 35, no. 1, pp. 65–85, 1999.
[2] J. P. Hespanha, M. Prandini, and S. Sastry, "Probabilistic pursuit-evasion games: A one-step nash approach," in *Proc. IEEE Conf. Decis. Control*, 2000, pp. 2272–2277.
[3] R. Vidal, O. Shakernia, H. Kim, D. Shim, and S. Sastry, "Probabilistic pursuit-evasion games: Theory, implementation, and experimental evaluation," *IEEE Trans. Robot. Autom.*, vol. 18, no. 5, pp. 662–669, Oct. 2002.
[4] S. D. Bopardikar, F. Bullo, and J. P. Hespanha, "On discrete-time pursuit-evasion games with sensing limitations," *IEEE Trans. Robot.*, vol. 24, no. 6, pp. 1429–1439, Dec. 2008.
[5] A. Pierson and M. Schwager, "Bio-inspired non-cooperative multi-robot herding," in *Proc. IEEE Int. Conf. Robot. Autom.*, 2015, pp. 1843–1849.
[6] A. Pierson and M. Schwager, "Controlling noncooperative herds with robotic herders," *IEEE Trans. Robot.*, vol. 34, no. 2, pp. 517–525, Apr. 2018.
[7] A. Pierson, Z. Wang, and M. Schwager, "Intercepting rogue robots: An algorithm for capturing multiple evaders with multiple pursuers," *IEEE Robot. Autom. Lett.*, vol. 2, no. 2, pp. 530–537, Apr. 2017.
[8] R. Licitra, Z. Hutcheson, E. Doucette, and W. E. Dixon, "Single agent herding of N-agents: A switched systems approach," in *Proc. IFAC World Congr.*, 2017, pp. 14374–14379.
[9] P. Deptula, Z. Bell, E. Doucette, W. J. Curtis, and W. E. Dixon, "Data-based reinforcement learning approximate optimal control for an uncertain

Authorized licensed use limited to: University of Florida. Downloaded on February 17,2026 at 23:10:35 UTC from IEEE Xplore. Restrictions apply.

nonlinear system with control effectiveness faults," *Automatica*, vol. 116, pp. 1–10, Jun. 2020.
[10] P. Deptula, Z. Bell, F. Zegers, R. Licitra, and W. E. Dixon, "Approximate optimal influence over an agent through an uncertain interaction dynamic," *Automatica*, vol. 134, pp. 1–13, Dec. 2021.
[11] R. Licitra, Z. I. Bell, E. Doucette, and W. E. Dixon, "Single agent indirect herding of multiple targets: A switched adaptive control approach," *IEEE Control Syst. Lett.*, vol. 2, no. 1, pp. 127–132, Jan. 2018.
[12] R. Licitra, Z. Bell, and W. Dixon, "Single agent indirect herding of multiple targets with unknown dynamics," *IEEE Trans. Robot.*, vol. 35, no. 4, pp. 847–860, Aug. 2019.
[13] A. Pierson, A. Ataei-Esfahani, I. Paschalidis, and M. Schwager, "Cooperative multi-quadrotor pursuit of an evader in an environment with no-fly zones," in *Proc. IEEE Int. Conf. Robot. Autom.*, 2016, pp. 320–326.
[14] E. Sebastián, E. Montijano, and C. Sagues, "Adaptive multirobot implicit control of heterogeneous herds," *IEEE Trans. Robot.*, vol. 38, no. 6, pp. 3622–3635, Dec. 2022.
[15] E. Sebastián and E. Montijano, "Multi-robot implicit control of herds," in *Proc. IEEE Int. Conf. Robot. Autom.*, 2021, pp. 1601–1607.
[16] A. Li, M. Ogura, and N. Wakamiya, "Swarm shepherding using bearing-only measurements," *Philos. Trans. A*, vol. 383, 2025, Art. no. 2289.
[17] B. Bennett and M. Trafankowski, "A comparative investigation of herding algorithms," in *Proc. Symp. Understanding Modelling Collective Phenomena*, 2012, pp. 33–38.
[18] N. K. Long, K. Sammut, D. Sgarioto, M. Garratt, and H. A. Abbass, "A comprehensive review of shepherding as a bio-inspired swarm-robotics guidance approach," *IEEE Trans. Emerg. Top. Comput. Intell.*, vol. 4, no. 4, pp. 523–537, Aug. 2020.
[19] J. Zhi and J. Lien, "Learning to herd agents amongst obstacles: Training robust shepherding behaviors using deep reinforcement learning," *IEEE Robot. Autom. Lett.*, vol. 6, no. 2, pp. 4163–4168, Apr. 2021.
[20] J. Zhi and J. Lien, "Learning to herd amongst obstacles from an optimized surrogate," in *Proc. IEEE/RSJ Int. Conf. Intell. Robots Syst.*, 2022, pp. 2954–2961.
[21] P. Deptula, Z. I. Bell, E. Doucette, J. W. Curtis, and W. E. Dixon, "Data-based reinforcement learning approximate optimal control for an uncertain nonlinear system with partial loss of control effectiveness," in *Proc. Am Control Conf.*, 2018, pp. 2521–2526.
[22] D. Strömbom et al., "Solving the shepherding problem: Heuristics for herding autonomous, interacting agents," *J. R. Soc. Interface*, vol. 11, no. 100, 2014, Art. no. 20140719.
[23] D. V. Dimarogonas, E. Frazzoli, and K. H. Johansson, "Distributed event-triggered control for multi-agent systems," *IEEE Trans. Autom. Control*, vol. 57, no. 5, pp. 1291–1297, May 2012.
[24] W. Heemels, K. Johansson, and P. Tabuada, "An introduction to event-triggered and self-triggered control," in *Proc. IEEE Conf. Decis. Control*, 2012, pp. 3270–3285.
[25] M. Mazo and P. Tabuada, "Decentralized event-triggered control over wireless sensor/actuator networks," *IEEE Trans. Autom. Control*, vol. 56, no. 10, pp. 2456–2461, Oct. 2011.
[26] W. Ren and R. W. Beard, *Distributed Consensus in Multi-Vehicle Cooperative Control*. Berlin, Germany: Springer, 2008.
[27] T. H. Cheng, Z. Kan, J. R. Klotz, J. M. Shea, and W. E. Dixon, "Event-triggered control of multi-agent systems for fixed and time-varying network topologies," *IEEE Trans. Autom. Control*, vol. 62, no. 10, pp. 5365–5371, Oct. 2017.
[28] P. Tabuada, "Event-triggered real-time scheduling of stabilizing control tasks," *IEEE Trans. Autom. Control*, vol. 52, pp. 1680–1685, Sep. 2007.
[29] D. V. Dimarogonas and K. H. Johansson, "Event-triggered cooperative control," in *Proc. Eur. Control Conf.*, 2009, pp. 3015–3020.
[30] D. P. Borgers and W. Heemels, "On minimum inter-event times in event-triggered control," in *Proc. IEEE Conf. Decis. Control*, 2013, pp. 7370–7375.
[31] J. Berneburg and C. Nowzari, "Robust dynamic event-triggered coordination with a designable minimum interevent time," *IEEE Trans. Autom. Control*, vol. 66, no. 8, pp. 3417–3428, Aug. 2021.
[32] C. Nowzari, E. Garcia, and J. Cortés, "Event-triggered communication and control of networked systems for multi-agent consensus," *Automatica*, vol. 105, pp. 1–27, 2019.
[33] P. Deptula, Z. I. Bell, F. Zegers, R. Licitra, and W. E. Dixon, "Single agent indirect herding via approximate dynamic programming," in *Proc. IEEE Conf. Decis. Control*, 2018, pp. 7136–7141.
[34] M. Bacon and N. Olgac, "Swarm herding using a region holding sliding mode controller," *J. Vib. Control*, vol. 18, no. 7, pp. 1056–1066, 2012.
[35] C. F. Nino, O. S. Patil, J. Philor, Z. Bell, and W. E. Dixon, "Deep adaptive indirect herding of multiple target agents with unknown interaction dynamics," in *Proc. IEEE Conf. Decis. Control*, 2023, pp. 2509–2514.
[36] H. K. Khalil, *Nonlinear Systems*, 3 ed. Englewood Cliffs, NJ, USA: Prentice Hall, 2002.

Authorized licensed use limited to: University of Florida. Downloaded on February 17,2026 at 23:10:35 UTC from IEEE Xplore. Restrictions apply.